Indian Journal of Pure & Applied Physics
Vol. 64, November 2026, pp. 1259-1271
DOI: 10.56042/ijpap.v64i11.34156

Numerical Investigation of Magnetised Sutterby Fluid Flow through a Porous Medium under Joule Heating and Chemical Reaction

Vinothkumar B[a*] & Revathi R[b]

[a]Department of Mathematics, Rajalakshmi Institute of Technology, Chennai 600 124, India
[b]Department of Mathematics, St Joseph University, Tamil Nadu 600 123, India

Received: 22nd July 2026; accepted: 12th October 2026

In the present work, the boundary-layer flow and heat–mass transfer of a non-Newtonian fluid of Sutterby type over a stretching sheet in a porous medium are investigated. The analysis accounts for significant physical phenomena such as Joule heating, thermal radiation, suction, internal heat generation, chemical reaction and Schmidt number for realistic transport phenomena found in industrial and engineering applications. The Sutterby fluid model is studied due to its capability to describe the nonlinear rheological properties such as shear-thinning and shear-thickening behaviour, which are important in polymer processing, coating technology, and thermal manufacturing systems. A uniform magnetic field is applied perpendicular to the direction of the stretching sheet and the porous medium resistance is incorporated to study the effect of porous medium on the fluid flow and heat transfer mechanism. Using appropriate similarity transformations, the governing set of nonlinear boundary-layer equations of momentum, temperature and concentration are transformed into a dimensionless set and subsequently solved numerically by the Keller–Box method. The influence of these parameters on the velocity, temperature and concentration profiles is explained in detail. The numerical results demonstrate that the fluid velocity is reduced by further increases in the magnetic field strength and the resistance of the porous medium, as a result of increased drag resistance. Thermal boundary layer thickness is greatly enhanced by thermal radiation, Joule heating, and heat generation. Increased Schmidt number and chemical reaction parameter decrease the concentration due to decreased mass diffusion. The momentum, thermal and concentration boundary layers are effectively reduced by suction. The current study is helpful for understanding the flow of Sutterby fluids in porous medium and has potential applications in thermal engineering and material processing.

Keywords: Sutterby fluid, Stretching sheet, Porous medium, Magnetic field, Joule heating, Schmidt number, Suction, Thermal radiation, Heat source, and Chemical reaction

1 Introduction

The study of the flow of non-Newtonian fluids over stretching surfaces has received considerable research interest due to its wide range of applications in polymer extrusion, wire drawing, coatings, food processing, biomedical engineering, thermal energy systems, etc. However, in many industrial processes, the rheological behaviour of highly viscous and shear-dependent liquids cannot be described by conventional Newtonian models. Thus, non-Newtonian models account for the complicated behaviour of these materials. Of these models, the Sutterby fluid model is an important rheological representation capable of modelling behaviour observed in polymeric melts, lubricants, biological suspensions, and industrial processing fluids. Because of these benefits, the Sutterby model is gaining significance in studies of heat and mass transfer associated with boundary-layer transport over deformable geometry.

Significant advances have been made in the last few years to understand Sutterby fluid flow over stretched, permeable surfaces[1]. It analysed the importance of magnetic force and velocity slip in Sutterby nanofluid flow over a rubber sheet and found that magnetic interaction has a significant effect on the momentum boundary layer, whereas the presence of nanoparticles influences the thermal field. When porous resistance was combined[2], it investigated the flow of Sutterby fluid over a stretched surface in porous media and found that porous resistance does affect the heat and concentration distributions significantly. Under Newtonian heating, the transport of Sutterby fluid in porous media under both electroosmotic and magnetohydrodynamic effects was modelled, and the importance of electromagnetic forcing in controlling fluid motion was highlighted. These investigations show the important practical

*Corresponding author: E-mail: vinoth.chk@gmail.com

relevance of the synergistic effect of using stretching surfaces and porous structures in thermal systems.

The extensive use of electrical conductivity in metallurgical operations, electronic cooling, magnetic drug targeting, solar collectors and chemical reactors has made the magnetohydrodynamic flow of such fluids through porous media a current research field. By investigating magnetised transport of microorganisms with gyro tactic properties over a cylindrical, Sarkar S & Das S[3] pointed out the strong coupling between fluid motion and thermal transport[4]. It used artificial neural network modelling for the transport of the magnetohydrodynamic Sutterby nanofluid, and demonstrated that data-driven prediction can be used to reasonably estimate the thermal performance. It has been[5] studied to investigate the heat transfer characteristics of the Sutterby hybrid nanofluid flow with consideration of the viscous dissipation and non-Fourier heat transport and found that thermal relaxation effects play a significant role on heat transfer characteristics. In a similar manner, Ali F et.al., and Abbas Z *et al*.,[6-7] have discussed the same and highlighted the sensitivity of temperature profiles to the nonlinear transport parameters in the case of rotation and radiation of Sutterby fluid. In addition, Ahmad W *et al*.,[8] showed that they have significant effects on the cylinder. Sutterby fluid studies were extended by Ramzan M *et al*., and Shahid A *et al*.,[9-10] on Darcy–Forchheimer porous structures and permeable surfaces where there were reductions in fluid velocity that were noticed. Shahid A *et al*.,[11] also studied in a permeable media and found that there was significant improvement in the transport of energy under activation energy conditions.

The effect of Sutterby fluid on thermal engineering applications of nanofluids and hybrid nanofluids has been also investigated by several authors. Kamel R S *et al*.,[12] numerically investigated transport of Sutterby nanofluid over a horizontal cylinder and found the enhancement of the surface heat transfer with the inclusion of nanoparticles. Usman A *et al*.,[13] studied the thermodynamic properties homogeneous–heterogeneous chemical reactions. Seada M M *et al.*,[14] investigated the solar heat applications nanofluid flowing over a stretching surface and found that the thermal efficiency of the hybrid nanofluid was enhanced. Sadiya A B *et al*.,[15] discussed the role of porous medium in ternary hybrid nanofluid transport over rotating stretching surfaces and Haider Q *et al*.,[16] discussed magneto-hydraulic transport over porous stretching surfaces. Abbas N et. al., and Ali M *et al*., [17-18] also indicated that the fluid transport by Sutterby over stretching geometries is very sensitive to thermophysical and diffusion parameters. The work[19-21] extended Sutterby's fluid dynamics to lubrication systems, electroosmotic transport and comparative convective heat transfer studies, respectively. Together, in works[22-28], it is found that the extension of surfaces under the action of porous drag and magnetic fields still represents a significant configuration in advanced non-Newtonian thermal transport.

In practical heat and mass transfer systems, all of the above are important physical mechanisms, as are absorption, suction, and the Schmidt number. In high-temperature applications, panels in aircraft or space, nuclear systems, and thermal manufacturing, radiation effects dominate. When fluid comes in contact with a magnetic field, joule heating adds extra thermal energy. Similarly, suction and porous injection are extensively used to control r and enhance the cooling effectiveness. Mechanisms of chemical reactions are also important in catalytic reactors, corrosion studies, biochemical diffusion and polymer synthesis. They noticed that the thermal enhancement was significant due to electrical dissipation. Narender G *et al*.,[29] investigated the modelling of the transport of MHD nanofluid in porous media with consideration of radiation and joule heating. Chemical reaction and Joule heating can greatly affect the concentration gradients of magnetised porous flow as reported[30]. On the other hand, Irfan M, Siddique I *et al*.,[31] investigated the effect of radiation and Joule heating on electroosmotic transport and Babu G S *et al*.,[32] focused on over porous plates. Kumar D *et al*., [33] illustrated the significance in addition to stretching-sheet geometry. It is clear from these studies that adding the two provides more realistic physical modelling.

Numerical solutions to highly nonlinear transformed boundary-layer equations need to be both accurate and stable. Of all the methods available in the literature, the Keller-Box method is known to be second-order accurate and unconditionally stable, with good convergence for nonlinear boundary-layer problems. It converts higher-order nonlinear differential equations into 1st-order systems, discretises them using a central finite-difference scheme, and numerically solves the resulting algebraic system using an iterative Newton linearization. The Keller–Box scheme is especially well suited for transport problems with coupled momentum,

thermal and concentration fields due to its robustness and efficiency[34]. Vinoth Kumar B *et al*.,[34] have successfully applied the KBM to study the flow of radiative nanofluid with a Lorentzian forcing and asymmetric heat source/sink. Its use for Jeffrey fluid flow over porous plates was further shown to be effective[35-36] . They used the KBM for the transport of; it was shown by Azad A *et al*.,[37] that the Keller–Box approach is accurate for nonlinear boundary value problems, and by Amigó *et al*.,[38] that Keller's mathematical framework is still important in computational analysis today. The contributions presented here have shown that the KBM is still one of the most reliable numerical techniques for nonlinear transport equations.

Fluid flow and heat transfer in porous media have received significant attention because of their applications in thermal engineering, energy systems, chemical processing, and industrial transport processes. The combined effects of magnetic fields, convection, porous structures, and frictional forces can considerably influence the flow and thermal characteristics. Revathi R *et al*.,[39] investigated magneto-convective flow through a permeable medium and highlighted the importance of suction and internal friction in controlling transport behavior.

Non-Newtonian fluids have attracted considerable interest because of their complex rheological characteristics. In particular, Sutterby and Williamson fluid models are widely employed to represent non-Newtonian flow behavior. Revathi R *et al*.,[40] studied mixed-convective Sutterby fluid flow with emphasis on thermal characteristics. Ahsan N *et al*.,[41] examined bioconvective Williamson fluid flow over a porous curved stretching surface with chemical reactions, demonstrating the importance of rheological, porous, and chemical effects on the flow and heat-transfer characteristics.

Magnetohydrodynamic (MHD) nanofluids have also gained considerable attention due to their enhanced thermal performance and controllability under an applied magnetic field. Vijayalakshmi N *et al*.,[42] investigated bioconvective MHD Williamson nanofluid flow over an inclined stretching surface considering viscous dissipation and Joule heating. Similarly, Jangid D *et al*.,[43] analyzed MHD Oldroyd-B nanofluid flow over a stretching sheet in porous media by incorporating melting, slip, radiation, and dissipative effects.

Chemical reactions and activation energy play an important role in many industrial and engineering processes involving heat and mass transfer. Sharma B K *et al*.,[44] studied MHD mixed-convective flow with higher-order chemical reactions and activation energy, while Ferdows M *et al*.,[45] examined the influence of chemical reaction order on boundary-layer flow with heat and mass transfer over a stretching sheet.

The above investigations demonstrate the importance of considering coupled physical effects in complex fluid-flow systems. Motivated by these studies, the present work investigates thermal, magnetic, porous, and/or chemical effects. The numerical results are used to analyse the flow, heat transfer, and mass transfer characteristics and to identify the influence of the governing parameters on the engineering quantities of interest.

A detailed study of the flow of Sutterby fluid over a stretching sheet, including the effects of a magnetic field, porous medium, thermal radiation, joule heating, non-uniform sink, suction, Schmidt number and chemical reaction simultaneously, is still limited in the available literature. These parameters interact in a highly nonlinear manner in boundary layers, which is crucial for advanced manufacturing processes, thermal energy management, polymer engineering, and transport in porous structures. The results of the above research will prove to be of value in thermal engineering applications of electrically conducting non-Newtonian fluids in porous industrial environments.

2 Methods and Materials

2.1 Mathematical Model

The physical setup of a 2-D boundary layer fluid over a continuous sheet in the presence of a uniform transversal MHD of strength B_0. is shown in Fig. 1. The sheet extends in the positive x-direction, and the y-axis is normal to the sheet. The extension of the sheet pulls the neighbouring fluid, creating a boundary layer where the velocity varies from the velocity at the wall to the velocity of the ambient fluid far away from the wall.

The momentum boundary layer is formed because of the viscous forces and is the region of the flow in which the velocity changes significantly. Beyond this layer, the fluid is essentially at rest. A thermal boundary layer is formed in such a way that the temperature varies from wall temperature to ambient temperature, $\widetilde{T}_\infty$. Likewise, the concentration boundary layer is formed by mass diffusion, as the

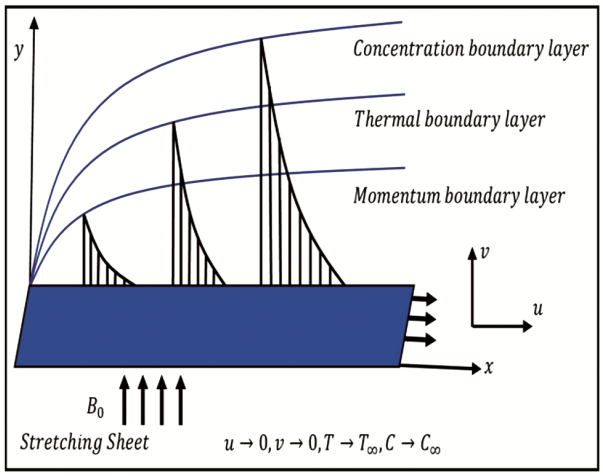

Fig. 1 — Flow model

concentration of the species tends towards the free-stream concentration $\tilde{C}_\infty$.

The arrows around the sheet indicate the stretching motion of the surface, and the coordinate system indicates the velocity components $\tilde{u}, \tilde{v}$ (along the x-direction) and (along the y-direction), the temperature is equal to the ambient temperature $(\tilde{T} \to \tilde{T}_\infty)$, and the concentration is equal to the ambient concentration$(\tilde{C} \to \tilde{C}_\infty)$.

Stress tensor of Sutterby fluid;

$$T = -pI + S \quad \dots (1)$$

$$S = \mu_0 \left[\frac{\sinh^{-1}(E\dot{\gamma})}{E\dot{\gamma}}\right]^m A_1 \quad \dots (2)$$

$$\dot{\gamma} = \sqrt{\frac{tr(A_1)^2}{2}} \quad \dots (3)$$

And

$$A_1 = (grade\, V) + (grad\, V)^T \quad \dots. (4)$$

$$\frac{\partial \tilde{u}}{\partial \tilde{x}} + \frac{\partial \tilde{v}}{\partial \tilde{y}} = 0 \quad \dots (5)$$

$$\tilde{u}\frac{\partial \tilde{u}}{\partial \tilde{x}} + \tilde{v}\frac{\partial \tilde{v}}{\partial \tilde{y}} = \frac{\mu}{\rho}\frac{\partial^2 \tilde{u}}{\partial \tilde{y}^2} + \frac{mA^2}{2}\left(\frac{\partial \tilde{u}}{\partial \tilde{y}}\right)^2\left(\frac{\partial^2 \tilde{u}}{\partial \tilde{v}^2}\right) - \frac{\sigma}{\rho}B_0^2\tilde{u} - \frac{\mu}{\rho k^*}\tilde{u} \quad \dots (6)$$

$$\tilde{u}\frac{\partial \tilde{T}}{\partial \tilde{x}} + \tilde{v}\frac{\partial \tilde{T}}{\partial \tilde{y}} = \frac{k}{\rho C_p}\frac{\partial^2 \tilde{T}}{\partial \tilde{y}^2} - \frac{1}{\rho C_p}\frac{\partial q_r}{\partial \tilde{y}} + \frac{Q_0}{\rho C_p}\left(\tilde{T} - \tilde{T}_\infty\right) + \frac{\mu}{\rho C_p}\left(\frac{\partial \tilde{u}}{\partial \tilde{y}}\right)^2 + \frac{\sigma B_0^2}{\rho C_p}\tilde{u}^2 \quad \dots (7)$$

$$\tilde{u}\frac{\partial \tilde{C}}{\partial \tilde{x}} + \tilde{v}\frac{\partial \tilde{C}}{\partial \tilde{y}} = D_B\frac{\partial^2 \tilde{C}}{\partial \tilde{y}^2} - k_r\left(\tilde{C} - \tilde{C}_\infty\right) \quad \dots (8)$$

The corresponding boundary conditions of the problem are;

$$\begin{aligned} &\tilde{u} = \tilde{U}_w, \tilde{v} = -\tilde{v}_w, \tilde{T} = \tilde{T}_w \\ &\tilde{C} = \tilde{C}_w \ \ at\ \tilde{y} = 0 \\ &\tilde{u} \to 0,\ \tilde{T} \to \tilde{T}_\infty \\ &\tilde{C} \to \tilde{C}_\infty \quad as\ \tilde{y} \to \infty \end{aligned} \quad \dots (9)$$

where, $\tilde{U}_w = cx$ for stretching the sheet with $c > 0$The contraction amount or expansion is held constant.

2.1.1 Similarity Transformations

$$\eta = \sqrt{\frac{c}{v}}y,\ \psi = xf(\eta)\sqrt{cv},\ \tilde{u} = \frac{\partial \psi}{\partial y},\ \tilde{v} = -\frac{\partial \psi}{\partial x}$$
$$\theta(\eta) = \frac{\tilde{T} - \tilde{T}_\infty}{\tilde{T}_W - \tilde{T}_\infty},\ \varphi(\eta) = \frac{\tilde{C} - \tilde{C}_\infty}{\tilde{C}_W - \tilde{C}_\infty} \quad (10)$$

where ψ is the stream function and η is a similarity variable. Based on the stream function we get,

$$\tilde{u} = \frac{\partial \psi}{\partial \tilde{y}} = \tilde{c}xf'(\eta),\ \tilde{v} = -\frac{\partial \psi}{\partial \tilde{x}} = -\sqrt{\tilde{c}v}f(\eta) \quad \dots (11)$$

2.1.2 Rosseland Approximation

$$\bar{q}_r = -\frac{4\sigma^*}{3k^*}\frac{\partial \tilde{T}^4}{\partial y} \quad \dots (12)$$

where,

$$\begin{aligned} &\tilde{T}^4 \cong 4\tilde{T}\tilde{T}_\infty^3 - 3\tilde{T}_\infty^3 \\ &\frac{\partial q_r}{\partial y} = \frac{16\sigma^*\tilde{T}_\infty^3}{3k^*\nu_f(\rho c_p)_f}\frac{\partial^2 \tilde{T}}{\partial y^2} \end{aligned} \quad \dots (13)$$

The Nusselt number Nu, Skin friction C_f coefficient and Sherwood number Sh are given as;

$$\begin{aligned} C_f &= \left(\frac{\tau_w}{\rho \tilde{U}_w^2}\right)_{\tilde{y}=0} \\ Nu &= \left(\frac{\tilde{x}q_w}{k(\tilde{T}_W - \tilde{T}_\infty)}\right) \\ Sh &= \left(\frac{\tilde{x}q_m}{D_B(\tilde{C}_W - \tilde{C}_\infty)}\right) \end{aligned} \quad \dots (14)$$

where

$$\tau_w = -\mu\left[\frac{\partial \tilde{u}}{\partial \tilde{y}} + \frac{m}{6}DeRe\left(\frac{\partial \tilde{u}}{\partial \tilde{y}}\right)^3\right]_{\tilde{y}=0}, q_w = -k\left[\frac{\partial \tilde{T}}{\partial \tilde{y}}\right]_{\tilde{y}=0}, q_m = -D_B\left[\frac{\partial \tilde{C}}{\partial \tilde{y}}\right]_{\tilde{y}=0}$$

Using the above similarity transformations, the Eqs. (2) - (4) are reduced to;

$$f'''\left[1+\frac{m}{2}\mathrm{Re}Def''^{2}\right]+ff''-(M+\lambda)f'-f'^{2}=0 \quad \ldots(15)$$

$$\frac{1}{\mathrm{Pr}}\left[1+\frac{4}{3}Nr\right]\theta''+Q\theta+f\theta'+\theta f'+Jf'^{2}+Ecf''^{2}=0 \quad \ldots(16)$$

$$\varphi''+Sc[f\varphi'-f'\varphi-Kr\varphi]=0 \quad \ldots(17)$$

The applicable boundary conditions (5) are converted to

$$f=0, f'=1,\ \theta=1,\ \varphi=1 \quad at\ \eta=0$$
$$f'=0,\ \theta=0,\ \varphi=0 \quad as\ \eta\to\infty \quad \ldots(18)$$

Where,

$$M=\frac{\sigma B_0^2}{\tilde{C}}, De=\frac{a^2A^2}{\nu}, \mathrm{Pr}=\frac{\mu c_p}{k}$$
$$Ec=\frac{\tilde{c}^2}{\nu(\tilde{T}_0-\tilde{T}_w)}, J=\frac{\tilde{c}x^2B_0^2}{(\tilde{T}_0-\tilde{T}_w)}$$
$$Nr=\frac{16\sigma^*T_\infty^3}{3k^*\nu f(\rho C_p)_f}, Sc=\frac{\nu}{D_B}, \mathrm{Re}=\frac{a^2}{\nu} \quad \ldots(19)$$
$$\lambda=\frac{\upsilon}{\mathrm{k}^*\tilde{C}}, \mathrm{Q}=\frac{Q_0}{a(\rho C_p)}$$

The Nusselt number (Nu), and C_f , and Sh,

$$Nu(\mathrm{Re})^{-\frac{1}{2}}=\left(1+\frac{4}{3}Nr\right)\theta'(0),$$
$$C_f\left((\mathrm{Re})^{-\frac{1}{2}}\right)=\left(f''(0)+\frac{m}{3}\mathrm{Re}De(f''(0)^3)\right) \quad \ldots(20)$$
$$Sh(\mathrm{Re})^{-\frac{1}{2}}=-\varphi'(0)$$

2.2 Numerical Method (Keller-Box Method)

2.2.1 Figure 2 Keller Box Method – Four-Step Procedure

Step 1 – First-order formulation The governing nonlinear differential equations are transformed into an equivalent system of first-order equations by introducing suitable auxiliary variables. The associated boundary conditions are also expressed in the transformed form.

Step 2 – Keller box discretisation The first-order system is discretised using the Keller Box finite-difference scheme. The computational domain is divided into a suitable mesh, and the equations are approximated at the midpoint of each mesh interval. This provides a second-order accurate implicit discretisation.

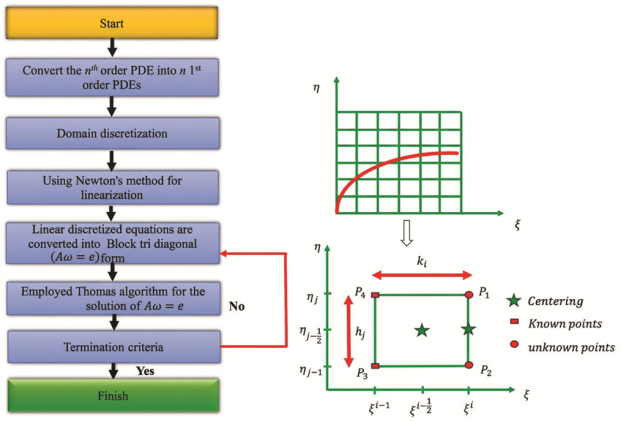

Fig. 2 ─ Keller box method

Step 3 – Newton linearization Because the discretised equations are nonlinear, Newton's linearization technique is employed. The nonlinear algebraic equations are converted into a sequence of linear systems by evaluating the Jacobian matrix about the current approximate solution.

Step 4 – Block-tridiagonal solution and convergence The resulting linearised equations form a block-tridiagonal system, which is solved efficiently using block elimination. The solution is iteratively updated until the prescribed convergence criterion is satisfied. In the present computation, a tolerance of (10^{-6}) is used to obtain a converged solution.

Figure 2 describes the computational sequence involved in the KBM for solving nonlinear boundary layer problems. The procedure begins by transforming the governing higher ODE into an equivalent system of first-order equations, which simplifies their numerical handling. The physical domain is then divided into a finite number of grid points, and finite difference approximations are applied within each small rectangular element of the mesh. Since the resulting equations are nonlinear, Newton's iterative technique is used to linearise the system at each step. This process generates a set of linear algebraic equations arranged in a block tri-diagonal matrix form. Such a structured system allows efficient computation and reduces numerical complexity. The linear system is subsequently solved using the Thomas algorithm, which is suitable for tridiagonal matrices. After obtaining the solution, a convergence test is performed to check whether the prescribed accuracy has been achieved. If the solution satisfies the termination criterion, the computation ends; otherwise, the iteration process is repeated until convergence is attained.

A grid-independence test was performed using progressively refined meshes, and the computed results showed negligible variation beyond the selected grid resolution. The computational domain was also varied to confirm domain independence and to ensure that the selected far-field boundary does not affect the numerical solution. Furthermore, the convergence tolerance was examined, and a tolerance of 10^{-6} was adopted to ensure stable and accurate convergence. These tests confirm that the numerical results obtained using the Keller Box Method are grid-independent, domain-independent, and satisfactorily converged

4 Results and Discussion

Table 1 shows the numerical values for the wall temperature gradient $(-\theta'(0))$ for some selected Prandtl number values and earlier published studies. This comparison is to check the correctness of the present numerical computation. The present value obtained is found to be very close to the reported values available in the literature, for each value of (Pr). There is only a slight difference in the number of results obtained from the present investigation and the previous investigations. This is evidence that the mathematical formulation and the numerical procedure used in the present analysis give an accurate solution. The comparison also illustrates the stable and consistent results obtained using the Keller–Box technique for the fluid flow over the previously mentioned stretching sheet in Sutterby. So, the present model can be confidently used to investigate thermal transport and concentration parameters. The physical behaviour of skin friction, heat transfer and mass transfer is presented in Table 2. Table 2 shows the physical behaviour of skin, heat and mass transfer. The variation of these three numbers with respect to the physical parameters of

Table 1 — Values of $-\theta'(0)$ for various values of Pr

Pr	Mukhopada [46]	Geetha [47]	Sujatha [48]	Present study	Error % approximations [46]	Error % approximations [47]	Error % approximations [48]
1	0.9547	0.95483	0.95406	0.9541	6 %	8 %	0.004 %
2	1.4714	1.47144	1.47145	1.4720	8 %	8 %	0.037 %
3	1.8961	1.89623	1.89537	1.8945	3 %	4 %	0.046 %

Table 2 — Skin friction, Nusselt number and Sherwood number

M	De	Re	m	λ	Nr	J	Ec	Q	Sc	Kr	S	Drag coefficient	Nusselt number	Sherwood number
0.1												-1.56962	5.46195	2.55008
0.3												-1.65002	5.35055	2.53951
0.5												-1.72669	5.24521	2.52976
0.7												-1.80018	5.14512	2.52071
1.0												-1.90537	5.00341	2.50824
	0.3											-1.65002	5.35055	2.53951
	1.0											-1.73016	5.36113	2.54070
	2.0											-1.84021	5.37492	2.54225
	3.0											-1.94602	5.38743	2.54367
	4.0											-2.04839	5.39891	2.54497
		1.0										-1.65002	5.35054	2.53951
		5.0										-1.75778	5.36820	2.54149
		9.0										-1.91467	5.38379	2.54325
		13										-2.03829	5.39781	2.54485
		17										-2.15773	5.41047	2.54629
			0.1									-1.65002	5.35055	2.53951
			0.7									-1.85096	5.37622	2.54240
			1.0									-1.94602	5.38743	2.54367
			1.5									-2.09848	5.40428	2.54558
			2.0									-2.24502	5.41923	2.54729
				0.1								-1.48476	5.58052	2.56161

(*Contd.*)

Table 2 — Skin friction, Nusselt number and Sherwood number (*Contd.)*

M	*De*	*Re*	*m*	λ	*Nr*	*J*	*Ec*	*Q*	*Sc*	*Kr*	*S*	Drag coefficient	Nusselt number	Sherwood number
				0.5								-1.65002	5.35054	2.53951
				0.9								-1.80018	5.14512	2.52071
				1.5								-2.00546	4.87033	2.49686
				2.0								-2.16312	4.66424	2.47989
					0.1							-1.65002	5.31561	2.53951
					0.3							-1.65002	5.31987	2.53951
					0.5							-1.65002	5.35054	2.53951
					0.7							-1.65002	5.39151	2.53951
					0.9							-1.65002	5.43521	2.53951
						0.1						-1.65002	5.90079	2.53952
						0.3						-1.65002	5.62566	2.53952
						0.5						-1.65002	5.35054	2.53952
						0.7						-1.65002	5.07545	2.53952
						0.9						-1.65002	4.80032	2.53952
							0.3					-1.65002	5.35054	2.53952
							0.5					-1.65002	4.63647	2.53952
							0.7					-1.65002	3.92240	2.53952
							0.9					-1.65002	3.20833	2.53952
							1.0					-1.65002	2.49426	2.53952
								0.2				-1.47275	3.17162	2.28758
								0.4				-1.58889	4.61117	2.45297
								0.6				-1.71315	6.09765	2.62857
								0.8				-1.36477	6.81464	2.13260
								1.0				-1.98529	7.10712	3.00901
									0.1			-1.65002	5.35054	0.62552
									0.2			-1.65002	5.35054	0.93472
									0.3			-1.65002	5.35054	1.19544
									0.4			-1.65002	5.35054	1.42734
									0.5			-1.65002	5.35054	1.63978
										0.1		-1.65002	5.35055	2.08429
										0.3		-1.65002	5.35055	2.22961
										0.5		-1.65002	5.35055	2.36100
										0.7		-1.65002	5.35055	2.48210
										0.9		-1.65002	5.35055	2.53951
											0.2	1.65002	4.90400	2.53952
											0.4	1.65002	5.79709	2.53952
											0.6	1.65002	6.69017	2.53952
											0.8	1.65002	7.58326	2.53952
											1.0	1.65002	8.47635	2.53952

the Sutterby fluid model over the stretching sheet is presented in Table 2. These are engineering quantities that represent the wall shear. The drag coefficient increases in magnitude with an increase in the magnetic field parameter (M) and the Nusselt number decreases slowly. This means that once the fluid begins to move, it will do so in a direction opposite to the magnetic force, thus increasing the resistance of the walls. Meanwhile, the Sherwood number varies only slightly. As the Deborah number (De) increases, the drag coefficient increases; both rates are gradually improved. This behaviour is a confirmation of the strong effect of the elastic property of the Sutterby fluid in strengthening the transport process. Correspondingly, a higher Reynolds number (Re) will result in higher wall shear and a slight improvement in both thermal and concentration transport. Results overall suggest that the geometry of the stretching

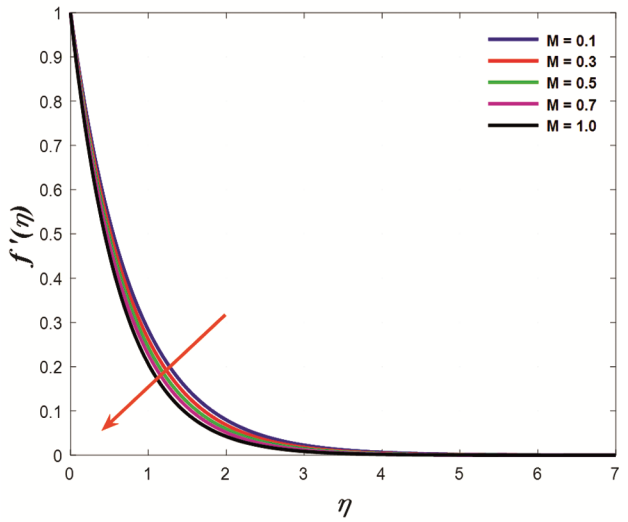

Fig. 3 — Effect of *M* on velocity

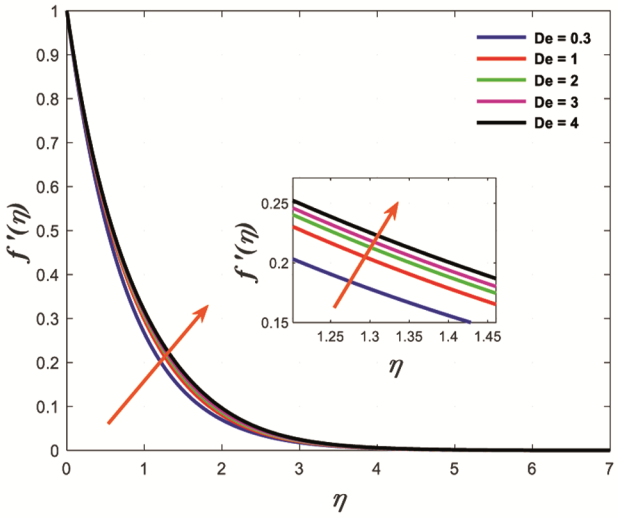

Fig. 4 — Effect of *De* on velocity

sheet is a dominant factor—along with magnetic and fluid elasticity effects—in the momentum, heat transfer, and species diffusion. These results are useful for understanding of the transport control in non-Newtonian thermal systems with Sutterby fluid flow in porous media.

The present graphical analysis shows the effect of the controlling parameters on the momentum and thermal transport of the Sutterby fluid over a continuously-stretched sheet embedded in a porous medium. This is a physical model where the sheet is stretched with a prescribed velocity in the axial direction, imparting momentum to the neighbouring fluid via the viscous interaction. The boundary layer, along with this stretching motion, magnetic force, porous resistance, thermal radiation and suction. The fluid velocity slowly reaches the free stream away from the sheet and the temperature decreases away from the heated wall to the ambient fluid. The response of the fluid under different physical parameters is explained below. To see how the velocity changes with the magnetic field parameter (m) (Fig. 3) The effect of magnetic field parameter (M) on dimensionless velocity profile is given in Fig. 3. As seen it is clear that the velocity of the fluid decreases with the increase of (M) all over the boundary-layer region. This behaviour is due to the fact that the applied transverse magnetic field causes an electromagnetic force, known as the Lorentz force. This force is in the opposite direction of flow and opposing flow caused by stretching. This in turn causes a reduction in momentum transport close to the wall and a faster decay of the velocity profile. The momentum boundary-layer thickness, therefore, becomes thinner for a larger magnetic parameter. Physically, this means that the magnetic field plays a key role in controlling the electrically conducting flow of Sutterby fluid over a stretching sheet, particularly in polymer coating and metallurgical transport systems. The velocity (Fig. 4) is affected by the Deborah number (De). The variation of velocity with different values of Deborah number is shown in Fig. 4. Larger (De) leads to a higher velocity. The Deborah number is the ratio of the elastic relaxation properties of the Sutterby fluid to the characteristic stretching time. The larger the Deborah number, the more elastic the response of the fluid particles. This means the fluid is pushed with a greater momentum from the stretching sheet, and is pushed to flow better on the surface. This means that the momentum boundary layer gets thicker. It is verified that the elasticity has a great influence on the fluid transportation in the Sutterby flow, and it cannot be neglected in the analysis of the non-Newtonian boundary-layer flow.

The effect of the magnetic field parameter (M) on the temperature (Fig. 5) It is found that the temperature distribution (M) is a continuous function of the magnetic strength and is shown in Fig. 5. While the magnetic field inhibits fluid motion, it also generates electrical resistance and internal dissipation converting some of the fluid's kinetic energy into thermal energy. This extra heat energy increases the temperature of the fluid in the vicinity of the

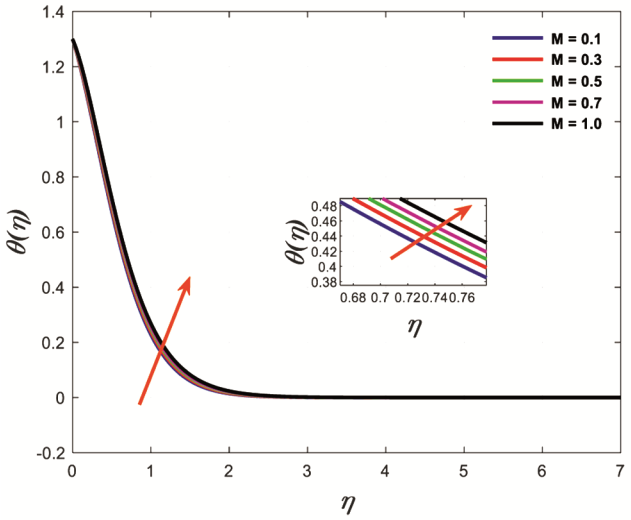

Fig. 5 — Effect of *M* on temperature

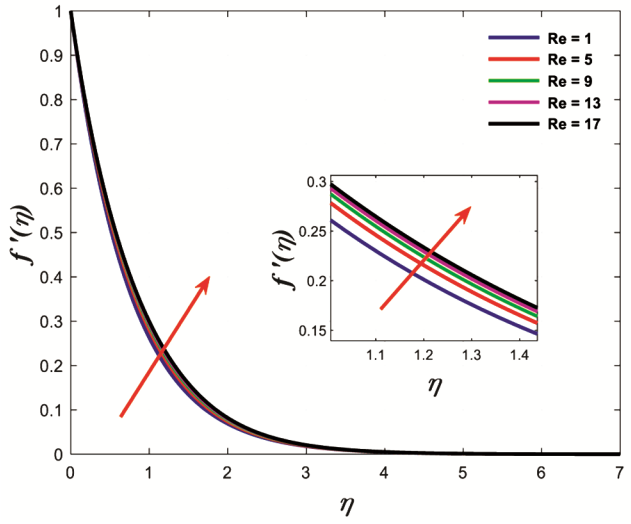

Fig. 6 — Effect of Re on velocity

stretching surface. Consequently, the thermal boundary layer increases in thickness and heat spreads deeper into the fluid region. This behavior is especially important for systems with magnetic control such as those generating thermal energy in an industrial system. The velocity as the Reynolds number (Re) changes (Fig. 6) As shown in Fig. 6, the velocity profile is higher for a higher Reynolds number. Reynolds number is the ratio between the inertial force and the viscous force. If (Re) becomes larger, the moving fluid will have more inertia than the viscous resistance. As a result, the fluid has less resistance to movement and it moves faster down the length of the stretching sheet. The momentum boundary layer thickens slightly, and the velocity of

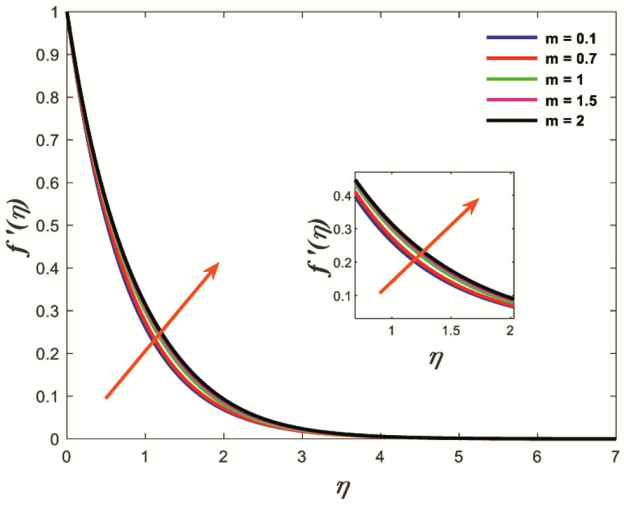

Fig. 7 — Effect of m on velocity

the fluid is not lost as far as the wall. This is consistent with the physical interpretation of increased momentum transport at high Reynolds number flows. The effect of porous medium parameter (m) on the velocity (Fig. 7). The impact of porous medium parameter is shown in Fig. 7. The velocity profile increases with increasing (m). The porous medium modifies the transfer of momentum between the stretching surface and the surrounding fluid. The more the permeability effect increases, the more fluid particles can flow through the porous area and the more momentum they can obtain from the stretching sheet. This results in a speed-up and lengthens the momentum boundary-layer thickness. The solution shows the significance of porous structures in the control of fluid transport in filtration, heat exchangers and porous thermal devices. The effects of the stretching parameter (λ) on the velocity are plotted in Fig. 8. The effect of the stretching parameter on the velocity is explained in Fig. 8. It is found that increasing (λ) decreases the velocity profile. The higher the length of stretch, the higher the wall shear and the stronger the velocity gradient in the vicinity of the sheet surface. This means that the fluid momentum diminishes faster from the wall with a thinner momentum boundary layer. This indicates that the rate of stretching is a major control of flow development across the sheet.

Variations in temperature (Fig. 9) due to the effect of the thermal radiation parameter (Nr) The temperature profile for various thermal radiation parameter values is shown in Fig. 9. There is a significant rise in temperature with the increase in

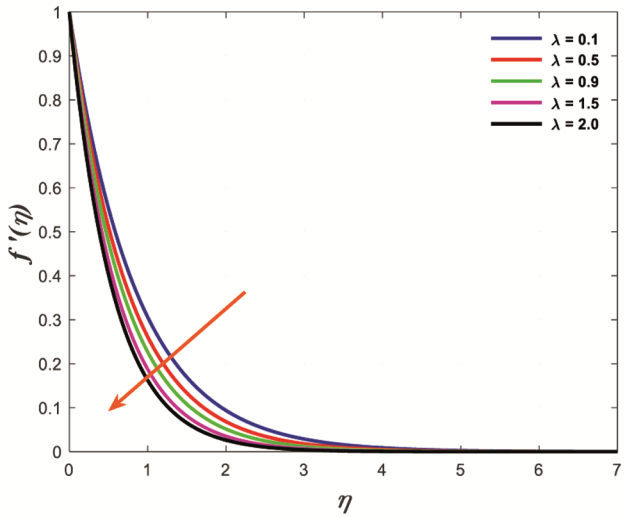

Fig. 8 — Effect of λ on velocity

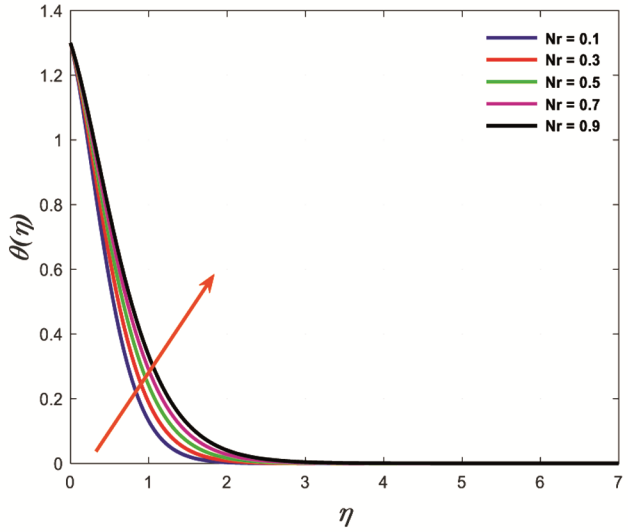

Fig. 9 — Effect of Nr on temperature

(Nr) is observed. Thermal radiation adds more heat energy to the fluid and promotes heat transfer from the stretching sheet. Hence, the temperature of the fluid is higher for a greater distance from the wall and the thickness of the thermal boundary layer increases. This behaviour is significant in high temperature engineering applications, such as solar thermal systems, polymer extrusion, glass production and radiative heat transfer processes. The effect of Eckert number (Ec) on temperature (Fig. 10) The results of temperature variation for various values of Eckert number (Ec) is shown in Fig. 10. It is noted that the temperature distribution is increased with the increase of (Ec). The Eckert number is a dimensionless parameter that represents the amount of kinetic energy

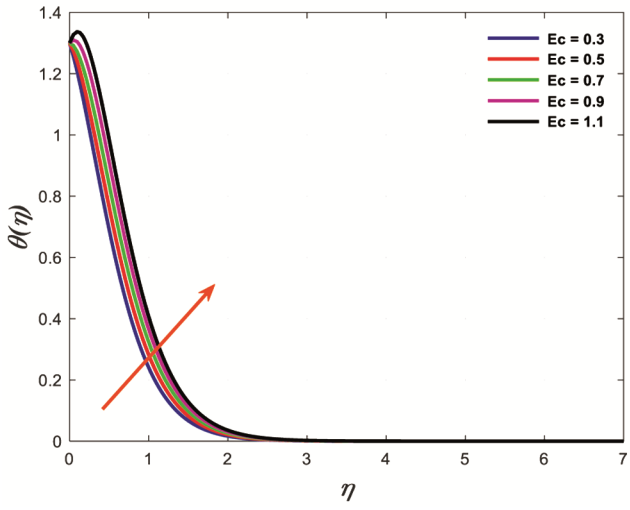

Fig. 10 — Effect of *Ec* on temperature

that is transformed to internal thermal energy due to viscous dissipation. As the speed of the fluid flow increases in the vicinity of the sheet, the friction between the fluid particles produces more heat. The heat is confined close to the The analysis shows that viscous dissipation plays a role in high-speed sheet stretching processes, and that it is a significant factor in enhanced heat transfer. The figure shows the effect of Q (heat source parameter) on the temperature (Fig. 11). The effect of internal heat generating parameter (Q) on temperature distribution is shown in Fig. 11. It is evident that the rise in (Q) increases the temperature profile profile over all the thermal boundary layer. A higher heat source parameter is equivalent to more heat added to the fluid region. The heat created within the system heats the fluid closer to the surface to be stretched, and the thermal energy goes deeper into the fluid. This causes the thermal boundary layer to thicken. It is physically significant in engineering systems where the material is heat-generating, the system is a thermal reactor, and energy is transferred by heat.

The effect of the stretch parameter (λ) on the temperature (Fig. 12) The effect of the stretching parameter on the temperature is indicated in Fig. 12. A temperature profile is becoming cooler as it moves toward the positive (λ). Increasing the stretching rate increases the velocity of the fluid near the wall, and thus decreases the amount of time for thermal diffusion to take place. This difference in time of contact results in less transfer of heat from the surface to the fluid and a drop in the fluid temperature. As a result, the thermal boundary layer is thinner. This

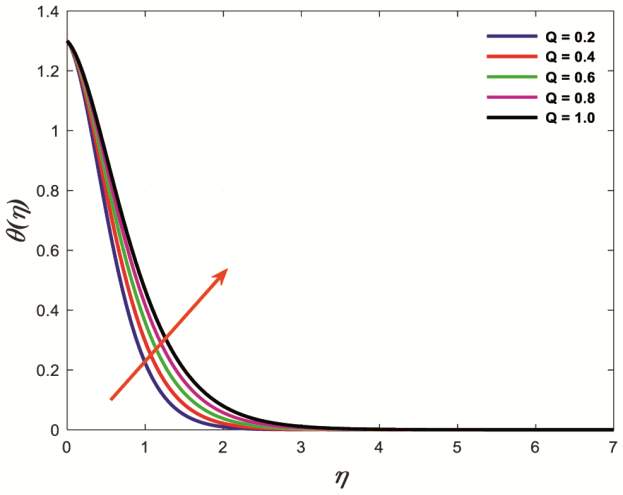

Fig. 11 — Effect of Q on temperature

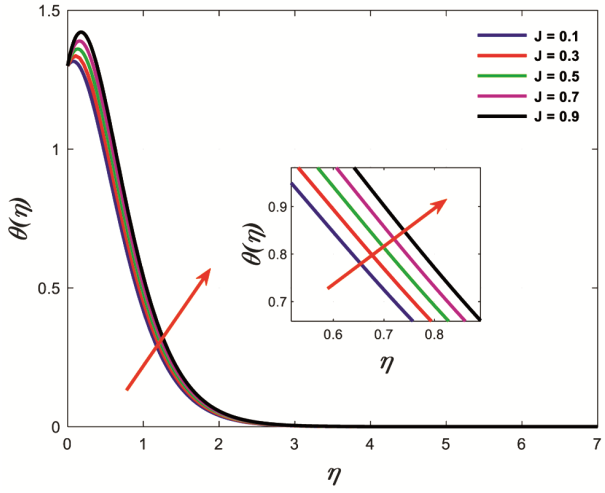

Fig. 13 — Effect of λ on temperature

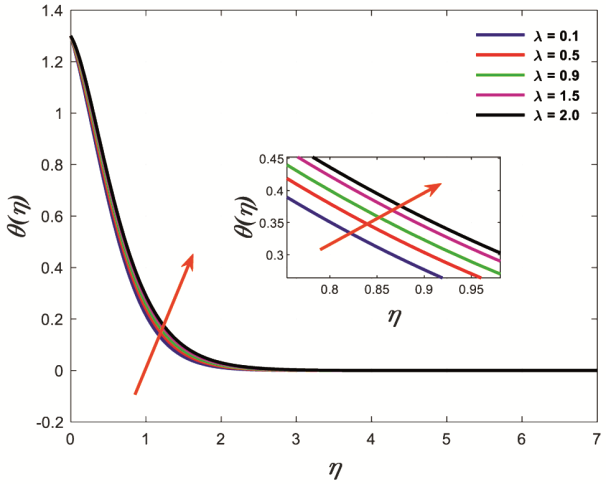

Fig. 12 — Effect of λ on temperature

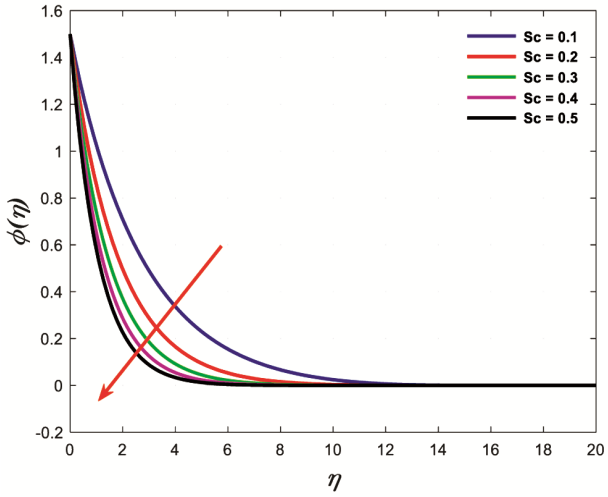

Fig. 14 — Effect of Sc on temperature

verifies that the surface heat transfer is controlled by stretching motion as an important mechanism. The result of the Joule heating parameter (J) on temperature (Fig. 13). The result is shown in Fig. 13, which exhibits the increase in temperature as the Joule heating parameter (J) increases. Joule heating is the heat produced by the electrical resistance of the electrically conducting fluid in the presence of a magnetic field. As (J) increases, the amount of heat energy increases. This will increase the fluid temperature and increase the thickness of the thermal boundary. The effect is greater near the stretching surface, where the electrical and thermal interactions are greatest. This observation is important in electromagnetic cooling systems and electrically conducting industrial fluids. The effect of Schmidt number (Sc) on concentration (Fig. 14). The distribution of concentration is influenced by Schmidt number (Sc) as shown in Fig. 14. As (Sc) increases, it is observed that the concentration decreases significantly. The higher the Schmidt number, the less effective is the molecular diffusion of species. Thus, the diffusion of concentration from the stretching sheet slows down, and the concentration boundary layer will be thinner. The concentration profile decreases quickly and is back to ambiance before. It is essential for chemical transport, diffusion-controlled reactions and mass transfer across stretching surfaces. The amount of chemical reaction parameter (Kr) effect on concentration (Fig. 15) In Fig. 15, the concentration variation with reaction parameter (Kr) is shown. As (Kr) increases, the concentration profile is decreasing. A more vigorous chemical reaction will use more species in the fluid, thus lowering the

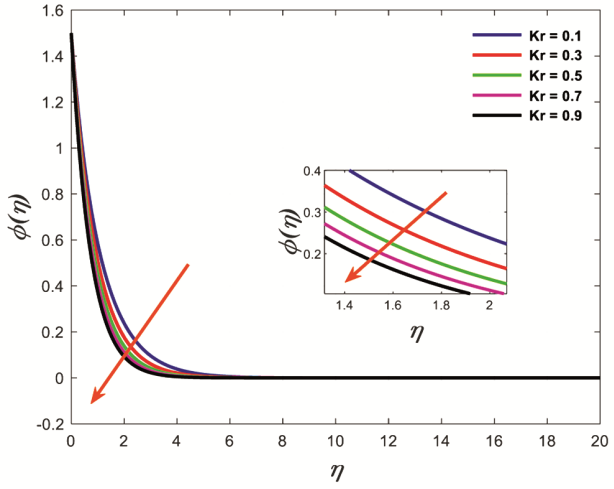

Fig. 15 — Effect of *Kr* on temperature

concentration around the stretching surface. Due to the higher consumption rate, the concentration boundary layer will be shallower, and concentration will attain zero value faster. This indicates that the mass transfer properties of reactive Sutterby fluid flow are well controlled by chemical reaction.

5 Conclusion

The present investigation supports the fact that the geometry of the stretching sheet greatly influences the momentum and heat transfer characteristics of the Sutterby fluid. The stretching motion sets the initial stage of boundary layer development and the controlling parameters control the transport properties. Magnetic field slows down the fluid movement while increasing temperature due to the resistance of the magnetic field. Increased velocity with fluid elasticity (Deborah number). Momentum transport is enhanced by the Reynolds number. A reduction in velocity and steadying of the boundary layer occur with suction. The addition of thermal radiation makes an important contribution to the thermal field. These results can be useful for the application of Sutterby fluids in polymer processing, coating flows, cooling of continuously moving sheets and for electrically conducting non-Newtonian fluids in thermal systems with porous environments. The results validate that the geometry of the stretching sheet has a significant effect on heat and mass transfer in the Sutterby fluid flow. The increase of Eckart number, heat source and joule heating increases the temperature due to more thermal energy generated within the fluid. The higher the stretching parameter, the lower the temperature, because the higher it is, the faster the fluids move, and the smaller the heat diffusion is. The Schmidt number and chemical reaction parameter decrease concentration since both lead to less species diffusion near the stretching surface. The observations give helpful physical insight in heat and mass transport phenomena in polymer extrusion, chemical processing, coating technology and thermal engineering systems that contain electrically conducting non-Newtonian fluids from the Sutterby type.

References

1 Srihari K, Shankar Goud B & Lokesh Babu T, *Results in Engineer*, 26 (2025) 105564.
2 Alrehili M, *Canad J Phys*, 103 (9) (2025) 901.
3 Sarkar S & Das S, *Inter J Model Simulation*, 45 (2) (2025) 387.
4 Ali F, Islam M, Ahmad F, Usman M & Asif S U, *Magnetochem* 11 (10) (2025) 88.
5 Awais, M, Kata S, Lakshmi R V, Afandi A, Garalleh H A & Rashid A A, *Results Surfaces and Interfaces*, 23 (2026) 100736.
6 Ali F, Kamal M, Faizan M & Zafar S S, *Modern Phys Lett B*, 39 (13) (2025) 2450471.
7 Abbas Z, Naeem A & Rafiq M Y, *J Radiat Res Appl Sci*, 18 (4) (2025) 102047.
8 Ahmad W, Rehman M I U, Hamid A & Hou M, *J Thermal Anal Calorim*, 150 (4) (2025) 2961.
9 Ramzan M, Alkhrijah Yazeed, Shahmir Nazia, Alazman Ibtehal, Saeed Abdulkafi Mohammed, Bilal Muhammad & Koh Wei Sin, *J Math*, 2025 (1) (2025) 8021103.
10 Shahid A, Hamid H B A, Shafique M, Khan H & Zhou H, *SSRN* 30 (2025) 5687708.
11 Shahid A, Miao Z, Mahmood A, Shafique M & Khan A, *Cogent Engineer* 12 (1) (2025) 2582949.
12 Kamel R S, Hady F M & Ismaeel A M, *Assiut University J Multidisciplin Sci Research*, 54 (2) (2025) 20.
13 Usman A & Khan W, *Bangmod Int J Math Comput Sci*, 11 (2025) 135.
14 Seada M M & Anwar S, *J Therm Anal Calorim*, 150 (22) (2025) 1.
15 Sadiya A B & Sucharitha G, *World J Eng*, 1 (2025) 1.
16 Haider Q, Sabir Z, Salahshour S, Ali M R, Eldin El S T & Sadat R, *Waves Random Complex Media*, 35 (7) (2026) 14492.
17 Abbas N, Shatanawi W & Shatnawi Taqi AM, *Canad J Phys*, 103 (4) (2025) 411.
18 Ali M, Abbas N & Shatanawi W, *Modern Phys Lett B*, 39 (14) (2025) 2450455.
19 Jazza Y, Hashim, Saqib M & Mousa S, *Sci Reports*, 16 (6477) (2026) 130.
20 Riasat S, Iqbal S, Bilal S, Ali M R & Flah A, *Nanofluid Flow*, (2025) 5120405.
21 Eswaramoorthi S, Loganathan K, Choudhary P, Senthilvadivu K, Ahlawat Anil & Sivakumar M, *Discover Appl Sci*, 7 (3) (2025) 159.
22 Aldhabani M S & Alrihieli H, *Case Studies Thermal Engineer*, 60 (2024) 104695.
23 Venkata Subba Rao M, Gangadhar K & Sobhana Babu P R, *Inter J Ambient Energy*, 43 (1) (2022) 5247.

24 Abbas N, Huda N U, Shatanawi W & Mustafa Z, *Modern Phys Lett B*, 38 (15) (2024) 2450085.
25 Bilal S, Shah I A, Akgül A, Tekin M T, Botmart T, Yousef E S & Yahia I S, *Alexandr Engineer J*, 61 (12) (2022) 11889.
26 Ishtiaq B, Nadeem S & Alzabut J, *Heliyon*, 9 (7) (2023) e17921.
27 Awan A U, Ahammad N A, Shatanawi W, Allahyani S Ay, Tag-ElDin E M, Abbas N & Ali Bagh, *Int Commun Heat Mass Transfer*, 139 (2022) 106399.
28 Duraihem F Z, *Modern Phys Lett B*, 39 (17) (2025) 2550019.
29 Narender G & Govardhan K, *Radiat Effects Defects Solids*, 180 (2026) 1.
30 Mng'ang'a J, *Inter J Math Math Sci*, 2023 (1) (2023) 9134811.
31 Irfan M, Siddique I, Gepreel K A, Nazeer M, Abduvalieva D & Khan M I, *Numeric Heat Transfer Part A: Appl*, 87 (1) (2024) 1.
32 Babu G S & Vijaya R B, *Multiscale Multidisciplin Model Experiments Design*, 8 (8) (2025) 373.
33 Kumar D, Sinha S, Sharma A, Agrawal P & Dadheech P K, *Heat Transfer*, 51 (2) (2022) 1939.
34 Vinoth Kumar B, Poornima T, Sreenivasulu P & Subba Rao A, *APL Mater*, 12 (2024) 041106.
35 Vinoth Kumar B & Poornima T, *Multiscale Multidiscip Model Exp Des*, 8 (2025) 359.
36 Tangsali P R, Katagi N N, Bhat A & Shettar M, *Cogent Eng*, 12 (1) (2025) 2555355.
37 Azad A, Yaghoubi E & Jafari A, *Comput Methods Differ Eq*, 12 (3) (2024) 425.
38 Amigó J M & Rosso O A, *Chaos*, 33 (8) (2023) 1.
39 Revathi R & Poornima T, *J Appl Phys*, 136 (2) (2024) 024701.
40 Revathi R & Poornima T, *J Therm Anal Calorim*, 149 (13) (2024) 7059.
41 Ahsan N, Alhowaity A, Abdelmohimen M A, Alrihieli H F & Al-Mdallal Q M, *Case Stud Therm Eng*, 68 (2025) 105924.
42 Vijayalakshmi N & Kumar P V, *J Therm Anal Calorim*, 10 (1) (2026) 1.
43 Jangid D, Jain P, Parmar A & Al-Mdallal Q, *Results Eng*, 27 (2025) 105950.
44 Sharma B K, Gandhi R, Mishra N K & Al-Mdallal Q M, *Sci Rep*, 12 (1) (2022) 17688.
45 Ferdows M & Al-Mdallal Q M, *Am J Fluid Dyn*, 2 (6) (2012) 89.
46 Mukhopadhyay S, *Alex Eng J*, 52 (3) (2013) 259.
47 Geetha R, Reddappa B, Tarakaramu N, Rushi Kumar B & Ijaz Khan M, *Int J Chem Eng*, 2024 (2024) 1.
48 Sujatha V & Sridhar W, *J Nav Archit Mar Eng*, 22 (1) (2025) 49.